

# Adsorption of SF<sub>6</sub> Decomposition Products by the S Vacancy Structure and Edge Structure of SnS<sub>2</sub>: A Density Functional Theory Study

Jincong Wang, Xiaoxing Zhang,\* Li Liu, and Zengting Wang



Cite This: *ACS Omega* 2021, 6, 28131–28139

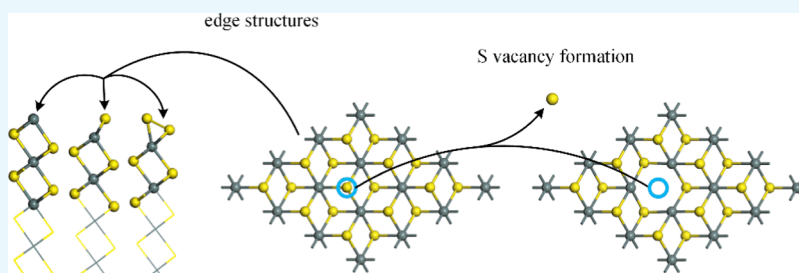


Read Online

ACCESS |

Metrics & More

Article Recommendations



**ABSTRACT:** Detecting the composition and concentration of SF<sub>6</sub> decomposition products is an effective method to evaluate the state of gas-insulated switchgear. Based on density functional theory, in this work we investigated the adsorption properties of four typical SF<sub>6</sub> decomposition products (H<sub>2</sub>S, SO<sub>2</sub>, SOF<sub>2</sub>, SO<sub>2</sub>F<sub>2</sub>) on an SnS<sub>2</sub> S vacancy structure (SnS<sub>2</sub>-S<sub>v</sub>) and SnS<sub>2</sub> edge structure (SnS<sub>2</sub>-edge). By calculating the adsorption energy, charge transfer, and comparing the density of states (DOS) of each system before and after the adsorption of gas molecules, the physical and chemical interactions between SnS<sub>2</sub> with different structures and gas molecules were investigated. The results show that SnS<sub>2</sub>-S<sub>v</sub> has the largest adsorption energy for SO<sub>2</sub> and has obvious chemical interactions. The S vacancy can effectively capture an O atom in SO<sub>2</sub>, causing SO<sub>2</sub> to firmly adsorb in the S vacancy. In addition, the adsorption of the four gases on the SnS<sub>2</sub>-edge is physical adsorption, in which the 50% S edge structure has the largest adsorption energy for H<sub>2</sub>S, reaching  $-0.52$  eV, and there is also a large charge transfer between the 50% S edge structure and H<sub>2</sub>S. Although the adsorption energy of SnS<sub>2</sub>-edge to the four gases is smaller than SnS<sub>2</sub>-S<sub>v</sub>, it is still greater than the pristine SnS<sub>2</sub>. This paper explores the adsorption properties of SnS<sub>2</sub>-S<sub>v</sub> and SnS<sub>2</sub>-edge for SF<sub>6</sub> decomposition products, providing insights for the development of SnS<sub>2</sub>-based gas sensors.

## 1. INTRODUCTION

In the power industry, sulfur hexafluoride (SF<sub>6</sub>) gas is a kind of insulating medium with good insulation performance and arc extinguishing performance, which has been widely used in gas insulating equipment. However, in practical engineering applications, there are inevitably some insulation defects in electrical equipment, such as metal burr, suspended conductive particles, etc. These defects will cause partial discharge<sup>1,2</sup> or partial overheating inside the equipment, which will lead to the decomposition of SF<sub>6</sub> gas and generate a series of low-fluoride sulfides (SF<sub>x</sub>,  $x = 1-5$ ). These low-fluoride sulfides easily react with microwater and micro-oxygen to produce HF, H<sub>2</sub>S, SO<sub>2</sub>, SOF<sub>2</sub>, SO<sub>2</sub>F<sub>2</sub>, and other gases.<sup>3-6</sup> These gases have a strong corrosive effect on the insulating materials or metal materials inside the equipment, which will accelerate the deterioration of insulation and eventually lead to the sudden breakdown of the equipment. Thus, the monitoring of SF<sub>6</sub> typical decomposition products can effectively carry out incipient fault diagnosis and ensure the stable operation of electrical equipment.

The carrier migration and heat diffusion of two-dimensional materials, such as graphene,<sup>12-14</sup> transition metal dichalcogenides (TMDCs),<sup>15,16</sup> MXenes,<sup>17,18</sup> hexagonal boron nitride,<sup>19,20</sup> etc., are confined to the two-dimensional plane,<sup>7-11</sup> which makes these materials exhibit many strange properties. Among them, TMDCs are MX<sub>2</sub>-type two-dimensional materials, where M is the transition metal (Mo, W, etc.) and X is the chalcogen (S, Se, Te). TMDCs are generally layered materials, and each layer of the repeating unit contains a layer of transition metal, which is added between two layers of S (Se, Te) atoms. The band gap of many TMDCs is in the range of 1–2 eV and increases as the number of layers

**Received:** August 6, 2021

**Accepted:** October 1, 2021

**Published:** October 13, 2021



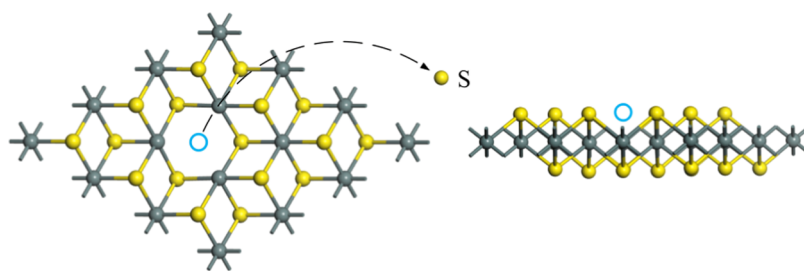


Figure 1.  $\text{SnS}_2\text{-S}_v$  structure.

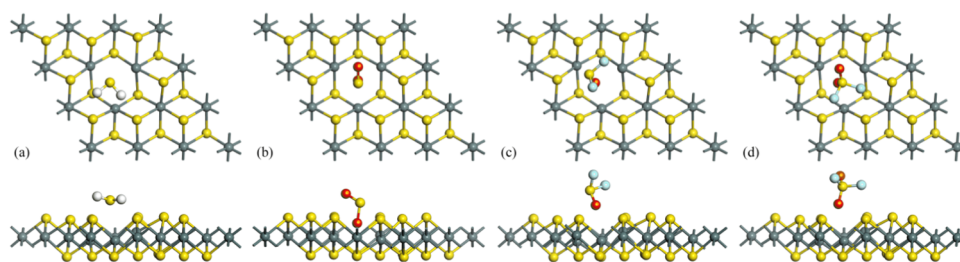


Figure 2. (a)  $\text{H}_2\text{S}$  adsorption system, (b)  $\text{SO}_2$  adsorption system, (c)  $\text{SOF}_2$  adsorption system, and (d)  $\text{SO}_2\text{F}_2$  adsorption system.

decreases. When the number of layers is reduced to a monolayer, the band structure also changes from the indirect band gap to the direct band gap. The unique band structure makes them very promising electronic and optical materials used in many precision devices. In addition, in the field of gas sensing, TMDCs have also received extensive attention due to their outstanding performance. The few-layer  $\text{MoS}_2$  nanosheets (FLMNs) prepared by mechanical exfoliation have excellent response and recovery performance to  $\text{NO}_2$  gas at room temperature.<sup>21</sup> Some scholars have also successfully prepared a low-cost and efficient  $\text{NH}_3$  gas sensor by using inkjet printing with high-concentration aqueous dispersion of  $\text{MoS}_2$ .<sup>22</sup> The  $\text{WS}_2$  nanoflake-based sensor shows an excellent response and good selectivity to  $\text{NH}_3$  at room temperature,<sup>23</sup> and the response will increase with the increase of humidity in the air. In theoretical calculation, some scholars found that  $\text{MoTe}_2$  had selectivity and sensitivity to  $\text{SO}_2$  in  $\text{SF}_6$  decomposition products based on first-principles calculation.<sup>24</sup> In addition, other  $\text{MX}_2$ -types of TMDCs also have excellent performance, such as  $\text{SnS}_2$ .  $\text{SnS}_2$  shows an excellent two-dimensional structure, with a band gap of 1.8 eV, an outstanding carrier mobility of  $50 \text{ cm}^2 \text{ V}^{-1} \text{ s}^{-1}$ , and a high on/off ratio, which has great application prospects in field-effect transistors.<sup>25,26</sup> In the field of gas sensing, some scholars use the liquid exfoliation method to detect low concentrations of the  $\text{NO}$  gas.<sup>27</sup> Other scholars prepared  $\text{SnS}_2$  by the high-energy ball-milling (HEBM) method with extremely high response to  $\text{NO}_2$  gas and reasonable response/recovery time.<sup>28</sup> The above research results indicate that  $\text{SnS}_2$  has potential as a gas-sensing material.

Under normal circumstances, in the exfoliation process of a monolayer, it will inevitably cause atomic detachment and form some vacancies, and these vacancies will significantly change the electronic properties of the material surface, enhance the chemical reaction, and improve its adsorption performance to gas molecules.<sup>29–32</sup> According to current reports, the chalcogen vacancies are the most easily formed defect.<sup>33,34</sup> In addition, some scholars have studied the interaction between the edge structure of TMDCs and gas molecules and found that the edge structure of TMDCs can

also effectively improve the adsorption performance of gas molecules.<sup>35</sup> Therefore, based on density functional theory, this work establishes the most stable adsorption model of  $\text{H}_2\text{S}$ ,  $\text{SO}_2$ ,  $\text{SOF}_2$ , and  $\text{SO}_2\text{F}_2$  on  $\text{SnS}_2\text{-S}_v$  and  $\text{SnS}_2$ -edge. We comprehensively investigated the interaction behavior between different  $\text{SnS}_2$  structures and  $\text{SF}_6$  decomposition products by calculating the adsorption energy, charge transfer, density of states, charge density difference, and recovery time. This work provides a theoretical basis for the application of gas sensors based on different  $\text{SnS}_2$  structures in the detection of  $\text{SF}_6$  decomposition products.

## 2. RESULTS AND DISCUSSION

### 2.1. Adsorption Analysis of $\text{SF}_6$ Decomposition Products on $\text{SnS}_2\text{-S}_v$ .

For TMDCs, the vacancy is usually an active site. In other words, the active site of  $\text{SnS}_2\text{-S}_v$  is the S vacancy, as shown in Figure 1. Therefore, in this paper, the adsorption sites of four  $\text{SF}_6$  decomposition products on  $\text{SnS}_2\text{-S}_v$  were set above the S vacancy, and the four molecules were made to approach the S vacancy from different angles. By comparing the adsorption energy, the most stable adsorption structures of the four gases on  $\text{SnS}_2\text{-S}_v$  were obtained. For the  $\text{H}_2\text{S}$  gas, three different initial adsorption structures can be set up,  $\text{H}_2\text{S}$  placed horizontally above the S vacancy or  $\text{H}_2\text{S}$  placed vertically with one of the H or S atoms placed above the S vacancy. The molecular structure of  $\text{SO}_2$  is similar to that of  $\text{H}_2\text{S}$ , both of which are V-shaped, and thus, the initial adsorption structure can be set up the same as that of  $\text{H}_2\text{S}$ .  $\text{SOF}_2$  gas has two initial adsorption structures, which are S atoms up/down close to S vacancies. The initial adsorption direction of  $\text{SO}_2\text{F}_2$  gas includes two kinds, one is the F atom near the S vacancy and the other is the O atom near the S vacancy.

The most stable adsorption structures of the four  $\text{SF}_6$  decomposition products on  $\text{SnS}_2\text{-S}_v$  are shown in Figure 2, and the adsorption energy, charge transfer, and adsorption distance are shown in Table 1.  $\text{H}_2\text{S}$  tends to be horizontally adsorbed to the vacancy of  $\text{SnS}_2\text{-S}_v$ , where the closest distances between H and S atoms and Sn atoms in  $\text{SnS}_2\text{-S}_v$  were 3.514 and 3.511 Å, respectively. It is worth noting that the six-

**Table 1.** SnS<sub>2</sub>-S<sub>v</sub> Adsorption Parameters

adsorption structure	adsorption energy (eV)	charge transfer (e)	adsorption distance (Å)
SnS <sub>2</sub> -S <sub>v</sub> /H <sub>2</sub> S	-0.69	0.0379	3.511 (S in H <sub>2</sub> S-Sn) 3.514 (H-Sn)
SnS <sub>2</sub> -S <sub>v</sub> /SO <sub>2</sub>	-1.11	-0.1963	3.545 (S in SO <sub>2</sub> -Sn) 2.458 (O-Sn)
SnS <sub>2</sub> -S <sub>v</sub> /SOF <sub>2</sub>	-0.63	0.0179	4.248 (S in SOF <sub>2</sub> -Sn) 3.236 (O-Sn)
SnS <sub>2</sub> -S <sub>v</sub> /SO <sub>2</sub> F <sub>2</sub>	-0.58	0.0277	4.198 (S in SO <sub>2</sub> F <sub>2</sub> -Sn) 3.291 (O-Sn)

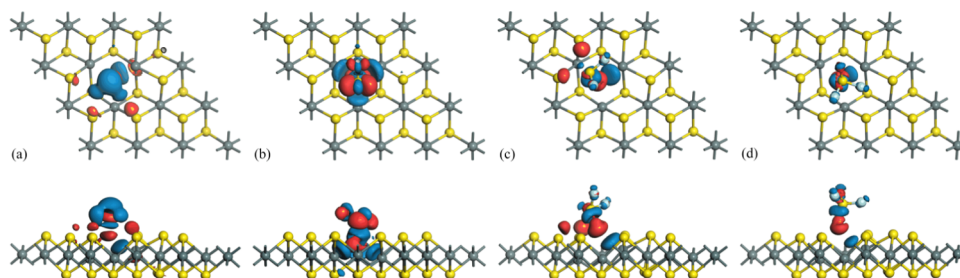
ring (Sn-S-Sn) below the S vacancy has a large deformation after adsorbing the H<sub>2</sub>S gas, and the Sn-S bond near H<sub>2</sub>S was shortened by 0.140 Å, and the Sn-S bond far away from H<sub>2</sub>S was extended by 0.269 Å. In addition, the adsorption energy of this structure is -0.69 eV. The larger deformation and adsorption energy means that there is a stronger interaction between H<sub>2</sub>S and SnS<sub>2</sub>-S<sub>v</sub>. Interestingly, when SnS<sub>2</sub>-S<sub>v</sub> adsorbs SO<sub>2</sub>, SO<sub>2</sub> will undergo a period of displacement and an O atom in SO<sub>2</sub> will enter the S vacancy. During this process, the SO<sub>2</sub> molecular structure also undergoes larger deformation. After the S-O bond enters the S vacancy, the bond length was stretched from 1.464 to 1.660 Å, and the bond angle of O-S-O was reduced from 119.7 to 109.3°. When the O atom enters the S vacancy, the distance to the Sn atom was only 2.458 Å. According to the displacement process of SO<sub>2</sub> and the deformation of SO<sub>2</sub> after entering the S vacancy, it is implied that a chemical interaction has occurred between SnS<sub>2</sub>-S<sub>v</sub> and SO<sub>2</sub>, and SnS<sub>2</sub>-S<sub>v</sub> can effectively capture O atoms in SO<sub>2</sub>. For SOF<sub>2</sub> and SO<sub>2</sub>F<sub>2</sub>, the adsorption mechanism is the same as that of SO<sub>2</sub>, in which O atoms tend to be close to the S vacancy in both. The six-ring under the S vacancy also undergoes a large deformation. This deformation is the same as that of the H<sub>2</sub>S adsorption system. The S-Sn bond close to the O atom was shortened, and the S-Sn bond far away from the O atom was extended.

Figure 3 shows the three-dimensional model diagram of the charge density difference (CDD), which will give a deeper understanding of the charge transfer between SnS<sub>2</sub>-S<sub>v</sub> and gas molecules. The red region is electron accumulation and the blue region is electron depletion. It is not difficult to find that the electron depletion mainly exists above H<sub>2</sub>S and above the Sn-S bond far away from H<sub>2</sub>S in the S vacancy. The electron accumulation mainly exists between the two H atoms of H<sub>2</sub>S, and partly exists above the S atoms on the surface of SnS<sub>2</sub>-S<sub>v</sub>. The adsorption of H<sub>2</sub>S will redistribute the electron to a certain extent. For the SO<sub>2</sub> adsorption system, the electron depletion exists on the S-O bond close to the S vacancy, which to a large extent weakens the strong interaction force

between the S atom and the O atom, resulting in the extension of the S-O bond length. However, far away from the S vacancy, there is no obvious electron depletion between the O atom and the S atom, so the bond length of the S-O bond far away from the S vacancy does not change significantly. For the two gases SOF<sub>2</sub> and SO<sub>2</sub>F<sub>2</sub>, the charge transfer mechanism is similar to the H<sub>2</sub>S adsorption system, both of which were obvious electron depletion above the Sn-n bond in the S vacancy; thus, the Sn-S bond was also extended. In summary, the electron in the four adsorption systems has been redistributed.

By calculating and comparing the changes of DOS before and after SnS<sub>2</sub>-S<sub>v</sub> adsorption of the four gases, the interaction between the four gases and SnS<sub>2</sub>-S<sub>v</sub> can be further explored. Figure 4a-d shows four adsorption systems, DOS, and PDOS (the lower part is DOS and the upper part is PDOS). In the H<sub>2</sub>S adsorption system, when SnS<sub>2</sub>-S<sub>v</sub> adsorbs H<sub>2</sub>S, the DOS will move to the right, the peak at 1 eV disappears, and a new peak appears at -14 eV. According to PDOS, the new peak is mainly related to the H 1s orbital. Moreover, from -6 to -2 eV, the S 3p orbital and the Sn 5p orbital have different degrees of overlap, and near 3 eV, the H 1s orbital, S 3p orbital, and Sn 5p orbital were almost completely overlapped, which indicates the existence of orbital hybridization, implying a strong interaction between SnS<sub>2</sub>-S<sub>v</sub> and H<sub>2</sub>S. In the SO<sub>2</sub> adsorption system, when SnS<sub>2</sub>-S<sub>v</sub> adsorbs SO<sub>2</sub>, new peaks appear at -12 and -6 eV. From -8 to -2 eV, and near the Fermi level (0 eV), the O 2p orbital, Sn 5s orbital, and Sn 5p orbital have a large area of overlap peaks, indicating that there is strong hybridization between O atoms and Sn atoms, which also supports the formation of new O-Sn bonds. Since in the adsorption mechanism of SOF<sub>2</sub> and SO<sub>2</sub>F<sub>2</sub> the O atom is close to the S vacancy, the hybridization between the orbitals is similar to the SO<sub>2</sub> adsorption system. From -7 to -4 eV, the Sn 5s orbital and Sn 5p orbital overlap with the O 2p orbital; however, the area of the overlapping peaks is smaller than that of the SO<sub>2</sub> adsorption system, therefore, the possibility of forming new chemical bonds is low.

**2.2. Adsorption Analysis of SF<sub>6</sub> Decomposition Products on the SnS<sub>2</sub>-edge.** The structure of SnS<sub>2</sub> is the 1T type. According to recent reports on the edge structure of 1T TMDCs,<sup>36</sup> three different edge structures have been established in this paper, as shown in Figure 5 the edge structure with 0% S covering atoms (0% S, 100% Sn); the edge structure with 50% S atom coverage (50% S, 50% Sn); the edge with a 100% S coverage structure (100% S, 0% Sn), respectively. After geometrically optimizing the three edge structures, considering the difference in the molecular structure



**Figure 3.** Charge density difference of the four adsorption systems: (a) H<sub>2</sub>S adsorption system, (b) SO<sub>2</sub> adsorption system, (c) SOF<sub>2</sub> adsorption system, and (d) SO<sub>2</sub>F<sub>2</sub> adsorption system (the isosurface of panels (a)–(d) is 0.005, 0.02, 0.005, and 0.005 e/Å<sup>3</sup>, respectively).

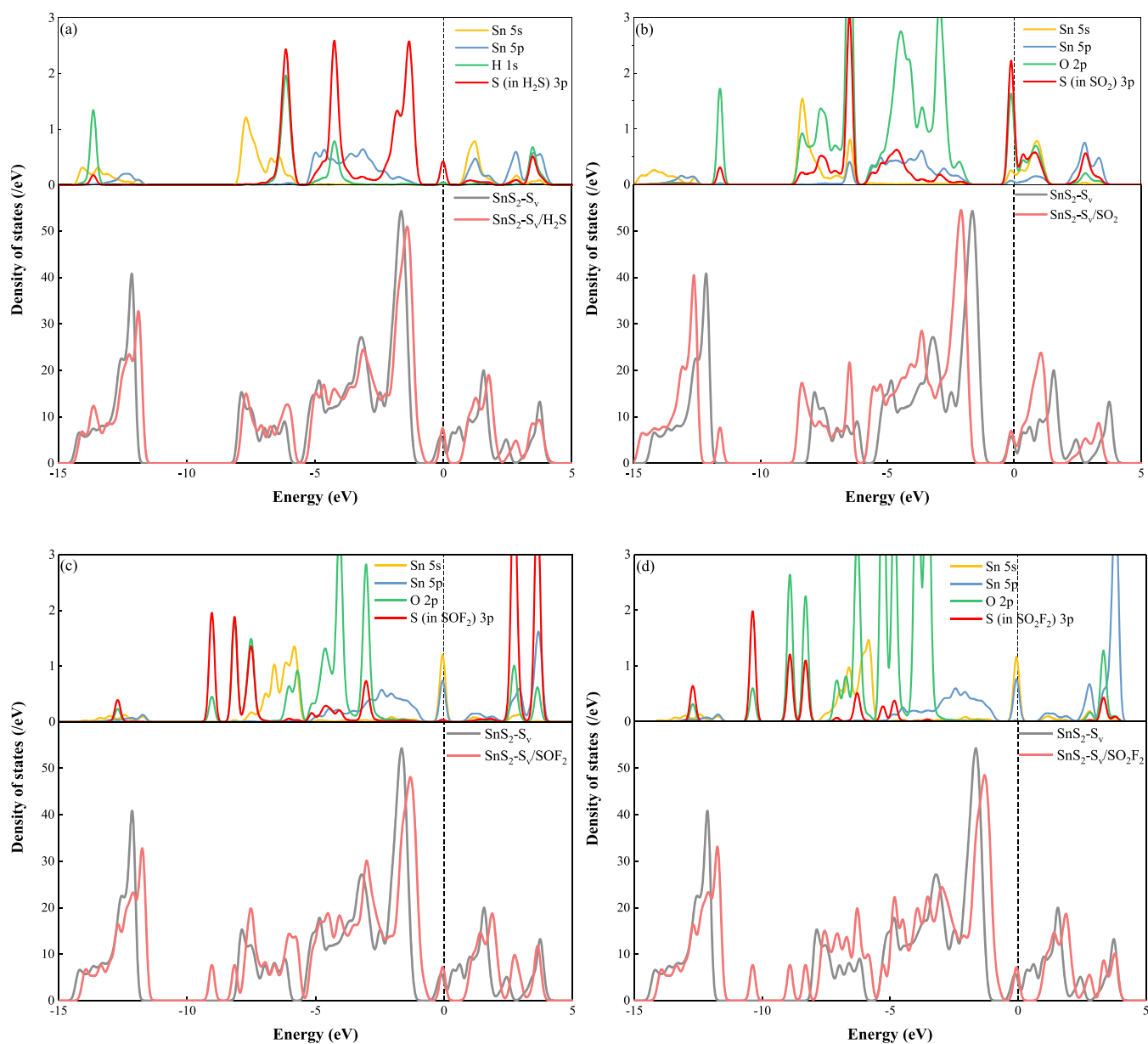


**Figure 4.** DOS and PDOS of the four adsorption systems: (a) H<sub>2</sub>S adsorption system, (b) SO<sub>2</sub> adsorption system, (c) SOF<sub>2</sub> adsorption system, and (d) SO<sub>2</sub>F<sub>2</sub> adsorption system.

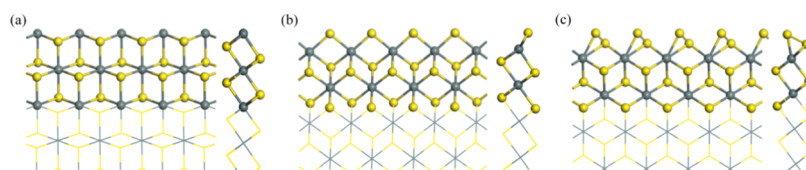


**Figure 5.** SnS<sub>2</sub>-edge structures: (a) 0% S structure, (b) 50% S structure, and (c) 100% S structure.

of each gas and the difference in the three edge structures, multiple adsorption systems were established.

Table 2 shows the adsorption energy, charge transfer, and adsorption distance of different adsorption systems. By comparing the adsorption energy in Table 2, it can be seen that among the three edge structures, the 50% S edge structure has better adsorption performance for the four gases, and the 100% S edge structure has weaker adsorption performance for the four gases than the other two edge structures. For the four gases, the adsorption performance of the three edge structures

for H<sub>2</sub>S is better than for the other three gases, and the adsorption energy of the 50% S edge structure for the H<sub>2</sub>S gas is the largest, reaching  $-0.52$  eV. In contrast, the three edge structures have weaker interactions with the two gases SOF<sub>2</sub> and SO<sub>2</sub>F<sub>2</sub>, and the adsorption energy is not higher than  $-0.3$  eV. When the four gas molecules are adsorbed on different edge structures, the charge transfer will be different. On the 0% S edge structure, SO<sub>2</sub> gains electrons and the other three gases lose electrons. On the 50% S edge structure, all four gases lose electrons. On the 100% S edge structure, H<sub>2</sub>S gains electrons,

**Table 2.** SnS<sub>2</sub>-S<sub>v</sub> Adsorption Parameters

adsorption structure	adsorption energy (eV)	charge transfer (e)	adsorption distance (Å)
0% S/H <sub>2</sub> S	-0.36	0.0399	2.745 (H-S in SnS <sub>2</sub> )
0% S/SO <sub>2</sub>	-0.34	-0.0185	3.193 (O-Sn)
0% S/SOF <sub>2</sub>	-0.28	0.0029	3.490 (O-Sn)
0% S/SO <sub>2</sub> F <sub>2</sub>	-0.23	0.0128	3.264 (O-Sn)
50% S/H <sub>2</sub> S	-0.52	0.1761	2.933 (S in H <sub>2</sub> S-Sn)
50% S/SO <sub>2</sub>	-0.37	0.0744	2.923 (O-Sn)
50% S/SOF <sub>2</sub>	-0.29	0.0221	2.945 (O-Sn)
50% S/SO <sub>2</sub> F <sub>2</sub>	-0.23	0.0440	3.127 (O-Sn)
100% S/H <sub>2</sub> S	-0.28	0.0652	2.687 (H-S in SnS <sub>2</sub> -edge)
100% S/SO <sub>2</sub>	-0.27	-0.0899	3.065 (S-S in SnS <sub>2</sub> -edge)
100% S/SOF <sub>2</sub>	-0.17	-0.0227	3.270 (F-S in SnS <sub>2</sub> -edge)
100% S/SO <sub>2</sub> F <sub>2</sub>	-0.18	-0.0009	3.414 (F-S in SnS <sub>2</sub> -edge)

and the other three gases lose electrons. Figure 6 shows the most stable adsorption structure and CDD of each adsorption system. According to the adsorption distance, it can be seen that the adsorption mechanisms of the three gases SO<sub>2</sub>, SOF<sub>2</sub>, and SO<sub>2</sub>F<sub>2</sub> tend to be in O atoms close to the 0% S edge structure and 50% S edge structure. According to CDD, it can be seen that except for the two adsorption systems of 100% S/SOF<sub>2</sub> and 100% S/SO<sub>2</sub>F<sub>2</sub>, all other adsorption systems have undergone electron redistribution.

We selected three structures with the largest adsorption energy for DOS analysis, namely, H<sub>2</sub>S adsorbed on the 0% S edge structure, 50% S edge structure, and 100% S edge structure, as shown in Figure 7. After the three edge structures adsorbed H<sub>2</sub>S, the DOS did not change significantly and there were only peak height differences in some positions. For the

0% S edge structure, the Sn 5s orbital and the S 3p orbital overlap significantly from -6 to -5 eV, and the Sn 5p orbital and the S 3p orbital have peak overlaps from -3 to 0 eV. For the 50% S edge structure, the Sn 5s orbital and S 3p orbital also have a large degree of peak overlap between -6 and -5 eV, while the Sn 5p orbital and S 3p orbital have a peak overlap between -5 and 0 eV. The degree of overlap is slightly greater than the 0% S edge structure, which also proves that the adsorption energy of H<sub>2</sub>S on the 50% S edge structure is greater than the 0% S edge structure. For the 100% S edge structure, the H 1s orbital, the S 3p orbital, and the Sn 5p orbital overlap between -5 and -3 eV, and the S 3p orbital and the Sn 5p orbital overlap slightly from -2.5 to 0 eV. In general, the three edge structures mainly interact with the S atoms in H<sub>2</sub>S.

### 2.3. Comparison of the Adsorption Performance of SF<sub>6</sub> Decomposition Products on Different Structures of SnS<sub>2</sub>

We calculated the adsorption energies of the four gases on pristine SnS<sub>2</sub> to evaluate whether SnS<sub>2</sub>-S<sub>v</sub> and SnS<sub>2</sub>-edge have improved adsorption properties for SF<sub>6</sub> decomposition products. The adsorption energies of H<sub>2</sub>S, SO<sub>2</sub>, SOF<sub>2</sub>, and SO<sub>2</sub>F<sub>2</sub> on pristine SnS<sub>2</sub> are -0.17, -0.18, -0.16, and -0.15 eV, respectively, which are consistent with the studies of other scholars<sup>37</sup> and also prove that our calculations are correct.

Figure 8 shows the comparison of the adsorption energies of the four gases on pristine SnS<sub>2</sub>, SnS<sub>2</sub>-S<sub>v</sub>, and SnS<sub>2</sub>-edge. It can be clearly seen that SnS<sub>2</sub>-S<sub>v</sub> can effectively improve the adsorption performance of the four gases, especially the adsorption of SO<sub>2</sub>. SnS<sub>2</sub>-edge can also improve the adsorption performance of the four gases to different degrees. The 0% S edge structure and 50% S edge structure can effectively improve the adsorption performance of H<sub>2</sub>S and SO<sub>2</sub>, among which the 50% S edge structure has the best adsorption performance for H<sub>2</sub>S. However, the adsorption performance of the four gases with the 100% S edge structure was not

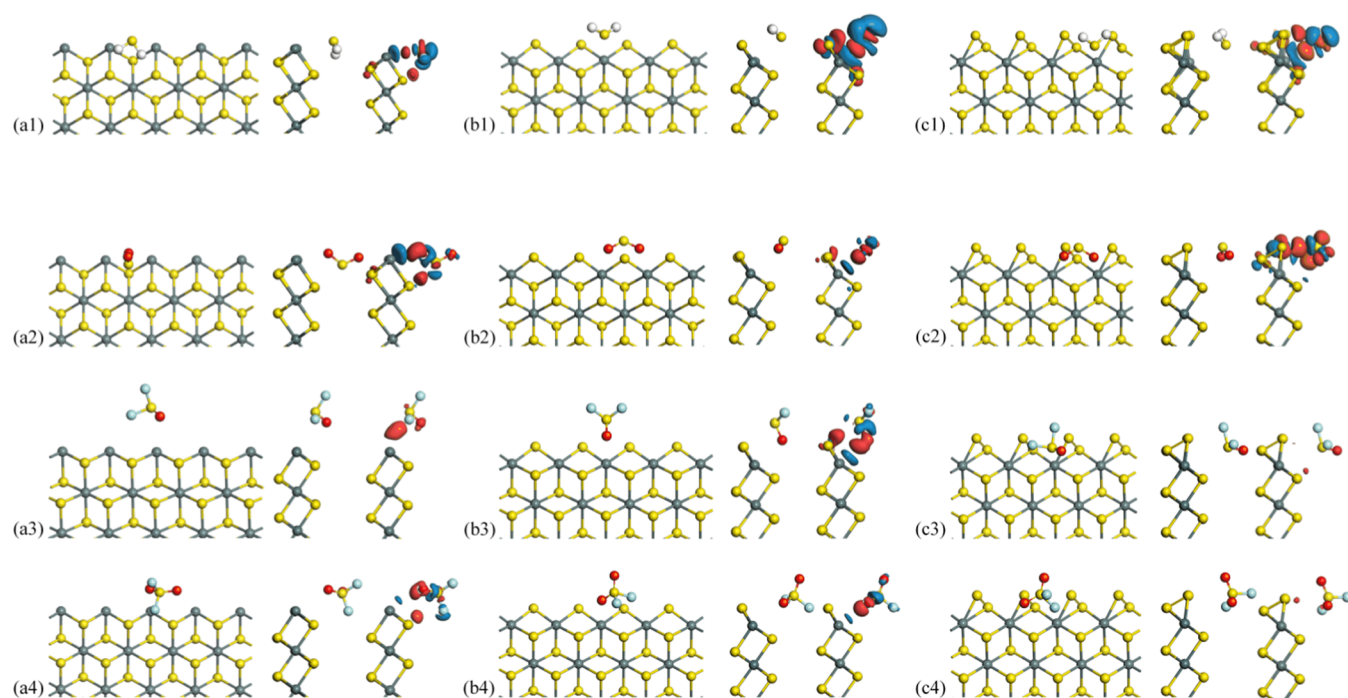


**Figure 6.** Adsorption structure and CDD (the isosurface is 0.005 e/Å<sup>3</sup>) of the four gases on the SnS<sub>2</sub>-edge (a1–a4) 0% S structure, (b1–b4) 50% S structure, and (c1–c4) 100% S structure.

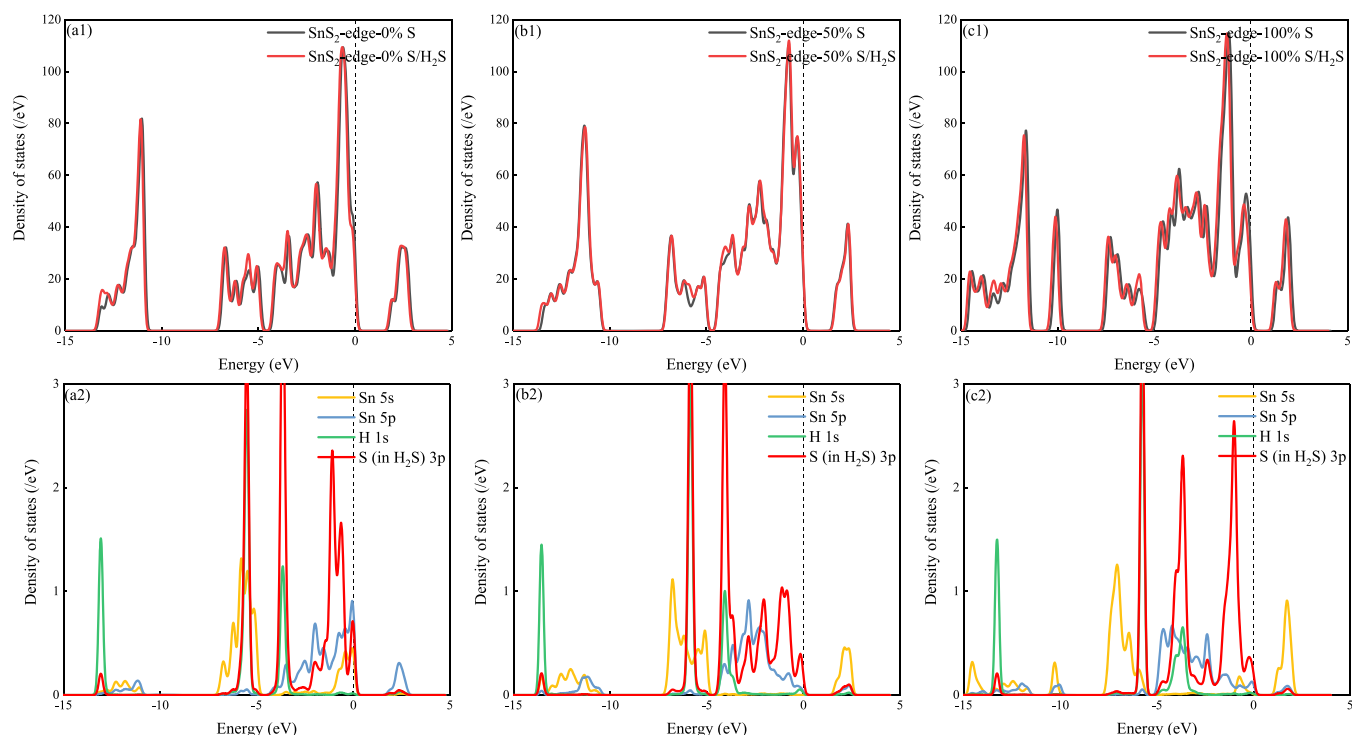


**Figure 7.** DOS and PDOS of H<sub>2</sub>S adsorption systems: (a1–a2) 0% S structure, (b1–b2) 50% S structure, and (c1–c2) 100% S structure.

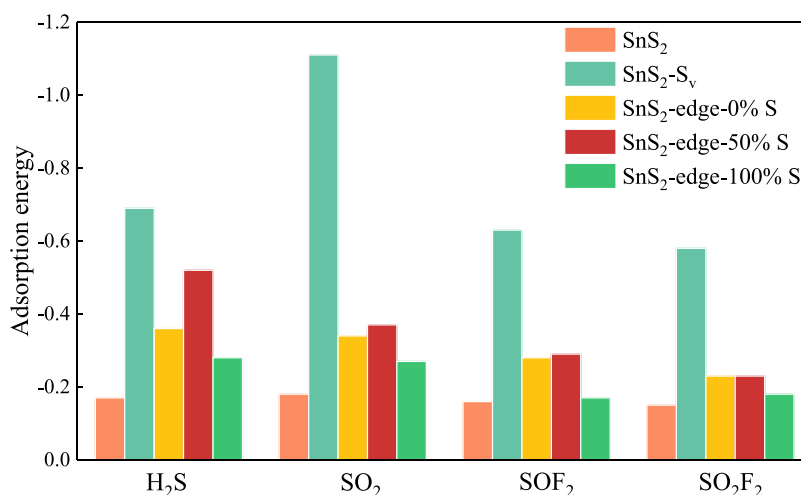


**Figure 8.** Comparison of the adsorption performance of the four gases on different structures of SnS<sub>2</sub>.

significantly improved, especially for SOF<sub>2</sub> and SO<sub>2</sub>F<sub>2</sub>. In general, SnS<sub>2</sub>-S<sub>v</sub> and SnS<sub>2</sub>-edge are beneficial to improve the adsorption performance of SF<sub>6</sub> decomposition products.

**2.4. Evaluation of the Values of SnS<sub>2</sub>-S<sub>v</sub> and SnS<sub>2</sub>-Edge as the Gas-Sensing Material to SF<sub>6</sub> Decomposed Products.** The value of SnS<sub>2</sub>-S<sub>v</sub> and SnS<sub>2</sub>-edge as gas-sensitive materials can be evaluated by the recovery time. The recovery time refers to the process of gas desorption from the sensor surface, which can be calculated by the van't Hoff Arrhenius equation.<sup>38</sup>

$$\tau = A^{-1} e^{(E_b/k_B T)} \quad (1)$$

where  $\tau$  is the recovery time;  $A$  is the attempt frequency factor, which is about  $10^{12}$  (s<sup>-1</sup>);<sup>39,40</sup> and  $E_b$  is the potential barrier that needs to be overcome for desorption, which is equal to the negative of the adsorption energy;  $k_B$  is the Boltzmann

constant; and  $T$  is the thermodynamic temperature. For the SnS<sub>2</sub>-edge, the 50% S/H<sub>2</sub>S adsorption system has the longest recovery time, which is about 619  $\mu$ s. The adsorption energy of other adsorption systems does not exceed  $-0.37$  eV, so the desorption time will be shorter. For SnS<sub>2</sub>-S<sub>v</sub>, when the SO<sub>2</sub> adsorption system works at 298 K, the recovery time is  $5.84 \times 10^5$  s, and when the temperature increases to 398 K, the recovery time is shortened to 112.54 s. In other words, when the temperature is in the range of 298–398 K, the recovery time of the SO<sub>2</sub> adsorption system can be adjusted between different orders of magnitude, which means that SnS<sub>2</sub>-S<sub>v</sub> is a promising gas-sensitive material for detecting SO<sub>2</sub>.

### 3. CONCLUSIONS

In this work, we considered the adsorption performance of SF<sub>6</sub> decomposition products on SnS<sub>2</sub>-S<sub>v</sub> and SnS<sub>2</sub>-edge. Based on

density functional theory, we calculated the adsorption energy, charge transfer, and differential charge density, and compared the DOS before and after the adsorption of gas molecules in each system and comprehensively investigated the physical and chemical interactions between gas molecules and SnS<sub>2</sub> with different structures. In addition, we also calculated the adsorption performance of the four gases on pristine SnS<sub>2</sub>, and compared the adsorption energy to evaluate whether the adsorption performance of SF<sub>6</sub> decomposition products on SnS<sub>2</sub>-S<sub>v</sub> and SnS<sub>2</sub>-edge can be improved. The results showed that the S vacancy of SnS<sub>2</sub>-S<sub>v</sub> can effectively capture the O atoms in SO<sub>2</sub>, SOF<sub>2</sub>, and SO<sub>2</sub>F<sub>2</sub>, and SO<sub>2</sub> will directly enter the S vacancy, causing the adsorption energy of the SO<sub>2</sub> adsorption system reach -1.11 eV, which is greater than those of the other three gases. In addition, SnS<sub>2</sub>-S<sub>v</sub> also has a suitable recovery time for SO<sub>2</sub>; when the temperature is 398 K, the recovery time is 112.54 s. SnS<sub>2</sub>-edge has three edge structures, which are the 0% S edge structure, 50% S edge structure, and 100% S edge structure. The three edge structures all have good adsorption properties for H<sub>2</sub>S, and there is a large charge transfer between the 50% S edge structure and H<sub>2</sub>S. However, the 100% S edge structure has weak adsorption of SOF<sub>2</sub> and SO<sub>2</sub>F<sub>2</sub>. By comparing the adsorption energies of the four gases on SnS<sub>2</sub>-S<sub>v</sub>, SnS<sub>2</sub>-edge and pristine SnS<sub>2</sub>, it can be found that SnS<sub>2</sub>-S<sub>v</sub> and SnS<sub>2</sub>-edge are beneficial to improve the adsorption performance of the four gases. Our research provides insights for the further development of SnS<sub>2</sub>-based gas sensors.

#### 4. COMPUTATIONAL METHODS

All geometric optimization and electronic calculations were based on the DMol<sup>3</sup> package.<sup>41</sup> The generalized gradient approximation (GGA) method and Perdew–Burke–Ernzerhof (PBE) functional were used to determine the electron exchange correlation function.<sup>42,43</sup> The double numerical polarization (DNP) was selected as the atomic orbital basis set and the DFT semicore pseudopotential (DSSP) was used to determine the relativistic effect of heavy elements.<sup>44</sup> The DFT-D2 method was used to determine the van der Waals force and long-range interactions.<sup>45</sup> The cutoff radius was set to 5.0 Å. For the geometric optimization of all structures, the convergence standard was set as follows: the energy difference between the two geometric optimization values was less than 1.0 × 10<sup>-5</sup> Ha, the force of each atom was less than 0.002 Ha/Å, and the maximum displacement distance of each atom was less than 0.005 Å.

The lattice parameter of bulk SnS<sub>2</sub> was calculated to be 3.69 Å. This is consistent with the research of other scholars.<sup>34,46</sup> By cleaving the (0 0 1) surface of bulk SnS<sub>2</sub>, a 3 × 3 × 1 single layer SnS<sub>2</sub> was established,<sup>47</sup> and the vacuum layer was set at 15 Å on the z-axis to avoid the interaction between adjacent layers. To simulate SnS<sub>2</sub> with the S vacancy, the perfect SnS<sub>2</sub> was geometrically optimized and then an S atom was removed (including 17 S atoms and 9 Sn atoms) and geometrically optimized again. For all geometrical optimizations, the Monkhorst Pack grid k-point in the Brillouin zone was set as 4 × 4 × 1, and a more accurate k-point of 8 × 8 × 1 was set for electronic calculations.

SnS<sub>2</sub> is a CdI<sub>2</sub> structure (1T structure) with the corresponding space group P3m1, and the Sn atom is octahedrally coordinated by the S atoms. The edge structure only exists on the (1 0 0) crystal plane,<sup>36</sup> and there are three different structures on the edge: 0% S atoms on the edge (0%

S, 100% Sn), 50% S atoms on the edge (50% S, 50% Sn), and 100% S atoms on the edge (100% S, 0% Sn). For the three edge structures, the repeat unit was set as the y-axis and there were four unit cells. The vacuum layer was set as 30 and 15 Å on the x-axis, and z-axis, respectively. The Monkhorst Pack grid k-point in the Brillouin zone was set as 1 × 3 × 1, and a more accurate k-point of 1 × 5 × 1 was set for electronic calculations.

Adsorption energy was used to characterize the adsorption properties of the four gas molecules on SnS<sub>2</sub>-S<sub>v</sub> or SnS<sub>2</sub>-edge. The calculation formula of the adsorption energy ( $E_{\text{ads}}$ )<sup>48,49</sup> can be defined as

$$E_{\text{ads}} = E_{\text{SnS}_2\text{-S}_v/\text{gas}} - E_{\text{SnS}_2\text{-S}_v} - E_{\text{gas}} \quad (2)$$

$$E_{\text{ads}} = E_{\text{SnS}_2\text{-edge}/\text{gas}} - E_{\text{SnS}_2\text{-edge}} - E_{\text{gas}} \quad (3)$$

where  $E_{\text{SnS}_2\text{-S}_v/\text{gas}}$  and  $E_{\text{SnS}_2\text{-edge}/\text{gas}}$  represent the total energy of the SnS<sub>2</sub>-S<sub>v</sub> adsorbed gas molecules and the total energy of the SnS<sub>2</sub>-edge-adsorbed gas molecules.  $E_{\text{SnS}_2\text{-S}_v}$  and  $E_{\text{SnS}_2\text{-edge}}$  represent the total energy of SnS<sub>2</sub>-S<sub>v</sub> and SnS<sub>2</sub>-edge.  $E_{\text{gas}}$  represents the total energy of gas molecules.

The charge transfer in each adsorption system was analyzed by the Hirshfeld method,<sup>50</sup> which is determined by the electron density.

$$Q = - \int \left( \frac{\rho_0(r)}{\sum \rho_0^T(r)} \right) (\rho(r) - \sum \rho_0^T(r)) dr \quad (4)$$

Here,  $\rho_0(r)$  represents the electron density in each atom's isolated state,  $\sum \rho_0^T(r)$  is the sum of  $\rho_0(r)$ , and  $\rho(r)$  represents the electron density of the entire system. The charge transfer ( $Q_T$ )<sup>51</sup> can be defined as

$$Q_T = Q_{\text{after}} - Q_{\text{before}} \quad (5)$$

where  $Q_{\text{after}}$  represents the electrons of gas molecules after adsorption and  $Q_{\text{before}}$  represents the electrons of gas molecules before adsorption. If the value of  $Q_T$  is positive, it indicates that during the adsorption process, the gas molecules lose electrons and the crystal gains electrons, and vice versa.

#### ■ AUTHOR INFORMATION

##### Corresponding Author

**Xiaoxing Zhang** – Hubei Engineering Research Center for Safety Monitoring of New Energy and Power Grid Equipment, Hubei University of Technology, Wuhan 430068, China; State Key Laboratory of Power Transmission Equipment & System Security and New Technology, Chongqing University, Chongqing 400044, China; [orcid.org/0000-0001-5872-2039](https://orcid.org/0000-0001-5872-2039); Email: [xiaoxing.zhang@outlook.com](mailto:xiaoxing.zhang@outlook.com)

##### Authors

**Jincong Wang** – Hubei Engineering Research Center for Safety Monitoring of New Energy and Power Grid Equipment, Hubei University of Technology, Wuhan 430068, China

**Li Liu** – Hubei Engineering Research Center for Safety Monitoring of New Energy and Power Grid Equipment, Hubei University of Technology, Wuhan 430068, China

**Zengting Wang** – Hubei Engineering Research Center for Safety Monitoring of New Energy and Power Grid Equipment, Hubei University of Technology, Wuhan 430068, China

Complete contact information is available at:  
<https://pubs.acs.org/10.1021/acsomega.1c04210>

## Notes

The authors declare no competing financial interest.

## ACKNOWLEDGMENTS

This work was supported by the Key Research and Development Program of Hubei Province, China (No. 2020BAA022).

## REFERENCES

- (1) Tang, J.; Liu, F.; Meng, Q.; Zhang, X.; Tao, J. Partial Discharge Recognition through an Analysis of SF<sub>6</sub> Decomposition Products Part 2: Feature Extraction and Decision Tree-based Pattern Recognition. *IEEE Trans. Dielectr. Electr. Insul.* **2012**, *19*, 37–44.
- (2) Tang, J.; Liu, F.; Zhang, X.; Meng, Q.; Zhou, J. Partial Discharge Recognition through an Analysis of SF<sub>6</sub> Decomposition Products Part 1: Decomposition Characteristics of SF<sub>6</sub> under Four Different Partial Discharges. *IEEE Trans. Dielectr. Electr. Insul.* **2012**, *19*, 29–36.
- (3) Sauers, I.; Ellis, H. W.; Christophorou, L. G. Neutral Decomposition Products in Spark Breakdown of SF<sub>6</sub>. *IEEE Trans. Electr. Insul.* **1986**, *EI-21*, 111–120.
- (4) Sauers, I. By-product formation in spark breakdown of SF<sub>6</sub>/O<sub>2</sub> mixtures. *Plasma Chem. Plasma Process.* **1988**, *8*, 247–262.
- (5) Dourdour, A.; Casanovas, J.; Grob, R.; Mathieu, J. Spark decomposition of SF<sub>6</sub>/H<sub>2</sub>O mixtures. *IEEE Trans. Electr. Insul.* **1989**, *24*, 1147–1157.
- (6) Beyer, C.; Jenett, H.; Klockow, D. Influence of reactive SF<sub>x</sub> gases on electrode surfaces after electrical discharges under SF<sub>6</sub> atmosphere. *IEEE Trans. Dielectr. Electr. Insul.* **2000**, *7*, 234–240.
- (7) Tan, C.; Cao, X.; Wu, X.-J.; He, Q.; Yang, J.; Zhang, X.; Chen, J.; Zhao, W.; Han, S.; Nam, G.-H.; Sindoro, M.; Zhang, H. Recent Advances in Ultrathin Two-Dimensional Nanomaterials. *Chem. Rev.* **2017**, *117*, 6225–6331.
- (8) Hu, S.; Zhu, M. Ultrathin Two-Dimensional Semiconductors for Photocatalysis in Energy and Environment Applications. *ChemCatChem* **2019**, *11*, 6147–6165.
- (9) Song, X.; Hu, J.; Zeng, H. Two-dimensional semiconductors: recent progress and future perspectives. *J. Mater. Chem. C* **2013**, *1*, 2952–2969.
- (10) Wang, D.; Yang, A.; Lan, T.; Fan, C.; Pan, J.; Liu, Z.; Chu, J.; Yuan, H.; Wang, X.; Rong, M.; Koratkar, N. Tellurene based chemical sensor. *J. Mater. Chem. A* **2019**, *7*, 26326–26333.
- (11) Wang, X. H.; Wang, D. W.; Yang, A. J.; Koratkar, N.; Chu, J. F.; Lv, P. L.; Rong, M. Z. Effects of adatom and gas molecule adsorption on the physical properties of tellurene: a first principles investigation. *Phys. Chem. Chem. Phys.* **2018**, *20*, 4058–4066.
- (12) Li, Y.; Xu, L.; Liu, H.; Li, Y. Graphdiyne and graphyne: from theoretical predictions to practical construction. *Chem. Soc. Rev.* **2014**, *43*, 2572–2586.
- (13) Sun, P.; Wang, K.; Zhu, H. Recent Developments in Graphene-Based Membranes: Structure, Mass-Transport Mechanism and Potential Applications. *Adv. Mater.* **2016**, *28*, 2287–2310.
- (14) Huang, C.; Li, Y.; Wang, N.; Xue, Y.; Zuo, Z.; Liu, H.; Li, Y. Progress in Research into 2D Graphdiyne-Based Materials. *Chem. Rev.* **2018**, *118*, 7744–7803.
- (15) Chhowalla, M.; Shin, H. S.; Eda, G.; Li, L.-J.; Loh, K. P.; Zhang, H. The chemistry of two-dimensional layered transition metal dichalcogenide nanosheets. *Nat. Chem.* **2013**, *5*, 263–275.
- (16) Tan, C.; Zhang, H. Two-dimensional transition metal dichalcogenide nanosheet-based composites. *Chem. Soc. Rev.* **2015**, *44*, 2713–2731.
- (17) Jeon, M.; Jun, B.-M.; Kim, S.; Jang, M.; Park, C. M.; Snyder, S. A.; Yoon, Y. A review on MXene-based nanomaterials as adsorbents in aqueous solution. *Chemosphere* **2020**, *261*, No. 127781.
- (18) Zhang, Y.; Wang, L.; Zhang, N.; Zhou, Z. Adsorptive environmental applications of MXene nanomaterials: a review. *RSC Adv.* **2018**, *8*, 19895–19905.
- (19) Boroznin, S. V.; Zaporotskova, I. V.; Perevalova, E. V. Investigation of Oxidation in Boron-Containing Nanotubes. *Nanosci. Nanotechnol. Lett.* **2012**, *4*, 1096–1099.
- (20) Sha, H.; Faller, R. A quantum chemistry study of curvature effects on boron nitride nanotubes/nanosheets for gas adsorption. *Phys. Chem. Chem. Phys.* **2016**, *18*, 19944–19949.
- (21) Li, W.; Zhang, Y.; Long, X.; Cao, J.; Xin, X.; Guan, X.; Peng, J.; Zheng, X. Gas Sensors Based on Mechanically Exfoliated MoS<sub>2</sub> Nanosheets for Room-Temperature NO<sub>2</sub> Detection. *Sensors* **2019**, *19*, No. 2123.
- (22) Yao, Y.; Tolentino, L.; Yang, Z.; Song, X.; Zhang, W.; Chen, Y.; Wong, C.-p. High-Concentration Aqueous Dispersions of MoS<sub>2</sub>. *Adv. Funct. Mater.* **2013**, *23*, 3577–3583.
- (23) Li, X.; Li, X.; Li, Z.; Wang, J.; Zhang, J. WS<sub>2</sub> nanoflakes based selective ammonia sensors at room temperature. *Sens. Actuators, B* **2017**, *240*, 273–277.
- (24) Wang, D.-W.; Wang, X.-H.; Yang, A.-J.; Chu, J.-F.; Lv, P.-L.; Liu, Y.; Rong, M.-Z. MoTe<sub>2</sub>: A Promising Candidate for SF<sub>6</sub> Decomposition Gas Sensors With High Sensitivity and Selectivity. *IEEE Electron Device Lett.* **2018**, *39*, 292–295.
- (25) Xu, L.; Zhang, P.; Jiang, H.; Wang, X.; Chen, F.; Hu, Z.; Gong, Y.; Shang, L.; Zhang, J.; Jiang, K.; Chu, J. Large-Scale Growth and Field-Effect Transistors Electrical Engineering of Atomic-Layer SnS<sub>2</sub>. *Small* **2019**, *15*, No. 1904116.
- (26) Song, H. S.; Li, S. L.; Gao, L.; Xu, Y.; Ueno, K.; Tang, J.; Cheng, Y. B.; Tsukagoshi, K. High-performance top-gated monolayer SnS<sub>2</sub> field-effect transistors and their integrated logic circuits. *Nanoscale* **2013**, *5*, 9666–9670.
- (27) Maria, K. H.; Sakhuja, N.; Jha, R. K.; Bhat, N. Ultra-Sonication Assisted Synthesis of 2D SnS<sub>2</sub> Nanoflakes for Room-Temperature No Gas Detection. *IEEE Sens. J.* **2021**, *21*, 10420–10427.
- (28) Kim, Y.-H.; Phan, D.-T.; Ahn, S.; Nam, K.-H.; Park, C.-M.; Jeon, K.-J. Two-dimensional SnS<sub>2</sub> materials as high-performance NO<sub>2</sub> sensors with fast response and high sensitivity. *Sens. Actuators, B* **2018**, *255*, 616–621.
- (29) Chee, S.-S.; Lee, J.-H.; Lee, K.; Ham, M.-H. Defect-Assisted Contact Property Enhancement in a Molybdenum Disulfide Monolayer. *ACS Appl. Mater. Interfaces* **2020**, *12*, 4129–4134.
- (30) Chen, Y.; Huang, S.; Ji, X.; Adepalli, K.; Yin, K.; Ling, X.; Wang, X.; Xue, J.; Dresselhaus, M.; Kong, J.; Yildiz, B. Tuning Electronic Structure of Single Layer MoS<sub>2</sub> through Defect and Interface Engineering. *ACS Nano* **2018**, *12*, 2569–2579.
- (31) Hu, Z.; Wu, Z.; Han, C.; He, J.; Ni, Z.; Chen, W. Two-dimensional transition metal dichalcogenides: interface and defect engineering. *Chem. Soc. Rev.* **2018**, *47*, 3100–3128.
- (32) Yang, A.; Wang, D.; Lan, T.; Chu, J.; Li, W.; Jianbin, P.; Liu, Z.; Wang, X.; Rong, M. Single ultrathin WO<sub>3</sub> nanowire as a superior gas sensor for SO<sub>2</sub> and H<sub>2</sub>S: Selective adsorption and distinct I-V response. *Mater. Chem. Phys.* **2019**, *240*, No. 122165.
- (33) Zhou, W.; Zou, X.; Najmaei, S.; Liu, Z.; Shi, Y.; Kong, J.; Lou, J.; Ajayan, P. M.; Yakobson, B. I.; Idrobo, J.-C. Intrinsic Structural Defects in Monolayer Molybdenum Disulfide. *Nano Lett.* **2013**, *13*, 2615–2622.
- (34) Cui, H.; Jia, P.; Peng, X.; Li, P. Adsorption and sensing of CO and C<sub>2</sub>H<sub>2</sub> by S-defected SnS<sub>2</sub> monolayer for DGA in transformer oil: A DFT study. *Mater. Chem. Phys.* **2020**, *249*, No. 123006.
- (35) Cho, S.-Y.; Kim, S. J.; Lee, Y.; Kim, J.-S.; Jung, W.-B.; Yoo, H.-W.; Kim, J.; Jung, H.-T. Highly Enhanced Gas Adsorption Properties in Vertically Aligned MoS<sub>2</sub> Layers. *ACS Nano* **2015**, *9*, 9314–9321.
- (36) Fu, L.; Wang, F.; Wu, B.; Wu, N.; Huang, W.; Wang, H.; Jin, C.; Zhuang, L.; He, J.; Fu, L.; Liu, Y. Van der Waals Epitaxial Growth of Atomic Layered HfS<sub>2</sub> Crystals for Ultrasensitive Near-Infrared Phototransistors. *Adv. Mater.* **2017**, *29*, No. 1700439.
- (37) Guo, S.; Hu, X.; Huang, Y.; Zhou, W.; Qu, H.; Xu, L.; Song, X.; Zhang, S.; Zeng, H. A highly sensitive and selective SnS<sub>2</sub> monolayer

sensor in detecting SF<sub>6</sub> decomposition gas. *Appl. Surf. Sci.* **2021**, *541*, No. 148494.

(38) Cui, H.; Liu, T.; Zhang, Y.; Zhang, X. Ru-InN Monolayer as a Gas Scavenger to Guard the Operation Status of SF<sub>6</sub> Insulation Devices: A First-Principles Theory. *IEEE Sens. J.* **2019**, *19*, 5249–5255.

(39) Patel, K.; Roonthe, B.; Dabhi, S. D.; Jha, P. K. A new flatland buddy as toxic gas scavenger: A first principles study. *J. Hazard. Mater.* **2018**, *351*, 337–345.

(40) Chen, D.; Zhang, X.; Tang, J.; Cui, Z.; Cui, H. Pristine and Cu decorated hexagonal InN monolayer, a promising candidate to detect and scavenge SF<sub>6</sub> decompositions based on first-principle study. *J. Hazard. Mater.* **2019**, *363*, 346–357.

(41) Li, P.; Hong, Q.; Wu, T.; Cui, H. SOF<sub>2</sub> sensing by Rh-doped PtS<sub>2</sub> monolayer for early diagnosis of partial discharge in the SF<sub>6</sub> insulation device. *Mol. Phys.* **2021**, *119*, No. e1919774.

(42) Perdew, J.; Burke, K.; Ernzerhof, M. Generalized Gradient Approximation Made Simple [Phys. Rev. Lett. *77*, 3865 (1996)]. *Phys. Rev. Lett.* **1997**, *78*, No. 1396.

(43) Delley, B. An All-Electron Numerical Method for Solving the Local Density Functional for Polyatomic Molecules. *J. Chem. Phys.* **1990**, *92*, 508–517.

(44) Delley, B. Hardness conserving semilocal pseudopotential. *Phys. Rev. B* **2002**, *66*, 1494.

(45) Grimme, S. Semiempirical GGA-Type Density Functional Constructed with a Long-Range Dispersion Correction. *J. Comput. Chem.* **2006**, *27*, 1787–99.

(46) Wang, X.; Wang, J. Effects of Pt and Au adsorption on the gas sensing performance of SnS<sub>2</sub> monolayers: A DFT study. *Mater. Sci. Semicond. Process.* **2021**, *121*, No. 105416.

(47) Cui, H.; Zhang, X.; Zhang, G.; Tang, J. Pd-doped MoS<sub>2</sub> monolayer: A promising candidate for DGA in transformer oil based on DFT method. *Appl. Surf. Sci.* **2019**, *470*, 1035–1042.

(48) Zhang, X.; Wang, J.; Chen, D.; Liu, L. The adsorption performance of harmful gas on Cu doped WS<sub>2</sub>: A First-principle study. *Mater. Today Commun.* **2021**, *28*, No. 102488.

(49) Zhang, X.; Cui, H.; Zhang, J.; Tang, J. Adsorption characteristic of Pd-4 cluster carbon nanotube towards transformer oil dissolved components: A simulation. *Appl. Surf. Sci.* **2017**, *419*, 802–810.

(50) Hirshfeld, F. Bonded-atom fragments for describing molecular charge densities. *Theor. Chim. Acta* **1977**, *44*, 129–138.

(51) Chen, D.; Zhang, X.; Tang, J.; Li, Y.; Cui, Z.; Zhou, Q. Using Single-Layer HfS<sub>2</sub> as Prospective Sensing Device Toward Typical Partial Discharge Gas in SF<sub>6</sub>-Based Gas-Insulated Switchgear. *IEEE Trans. Electron Devices* **2019**, *66*, 689–695.